Talanta 116 (2013) 852–859

Contents lists available at ScienceDirect

Talanta

journal homepage: www.elsevier.com/locate/talanta

Gold-nanoparticle-embedded nafion composite modified on glassy carbon electrode for highly selective detection of arsenic(III)

Jing-Fang Huang *, Hsiao-Hua Chen

Department of Chemistry, National Chung Hsing University, Taichung 402, Taiwan, R.O.C

ARTICLE INFO

Article history:
Received 25 June 2013
Received in revised form
24 July 2013
Accepted 25 July 2013
Available online 8 August 2013

Keywords:
Arsenic
Stripping voltammetry
Au nanoparticle
Composite
Nafion

ABSTRACT

A Cu(I)-ion-mediating Au reduction is proposed for preparing an Au-nanoparticle-embedded nafion (NF(Au_{nano})) composite. The NF(Au_{nano}) composite consisted of highly dense, well-dispersed, and protecting-agent-free Au nanocrystals with a narrow particle size (4.8 ± 0.1 nm) distribution. The NF(Au_{nano}) composite was characterized as a function of composition and particle size distribution using powder X-ray diffraction, transmission electron microscopy, and electrochemical measurements. It was demonstrated that the NF(Au_{nano}) composite provided high activity in the redox behavior of As(III), and was used as a potential sensing material with low Au loading for As(III) detection. An NF(Au_{nano})-composite-modified electrode is easy to prepare and regenerate. The dynamic range of a calibration curve from 0.1 to 12.0 $\mu g\,L^{-1}$ (from 1.3 to 160 nM), $y=23.98x$ (in $\mu A\,\mu M^{-1}$)+0.42 ($R^2=0.999$), showed linear behavior with a slope of 23.98 $\mu A\,\mu M^{-1}$. The detection limit is as low as 0.047 $\mu g\,L^{-1}$ (0.63 nM). The chelating agent ethylenediaminetetraacetate (EDTA) can selectively chelate with interfering metal ions, forming bulky complexes or bulky anions that are excluded from the NF film. The presence of EDTA effectively eliminated interference from several metal ions, particularly Cu(II) and Hg(II), which are generally considered to be major interferents in the electroanalysis of As(III). This method was applicable to As(III) analysis in three real water samples, namely groundwater, lake, and drinking waters.

1. Introduction

Because of their high toxicities, the determination of trace metal ions is of concern not only in environmental matrices, but also in biological materials [1–5]. Metal ions such as arsenic, copper, lead, cadmium, and mercury are important pollutants that can be present in foods, drinking water, and other beverages, and in aquatic environments [6–9]. Arsenic is a toxic substance. Inorganic arsenic contamination in drinking water is a serious worldwide threat to human health. Arsenite (As(III)) and arsenate (As(V)) are the inorganic forms found in groundwater and are more toxic than the organic forms, with As(III) being the most toxic [10–14]. Arsenic can cause a range of acute and chronic effects, including dermal changes and respiratory, cardiovascular, gastrointestinal, mutagenic, and carcinogenic effects after long-term exposure [10–14]. It has been reported that the pollution of groundwater from arsenic leads to adverse health effects in 20 countries. In these countries, arsenic levels in drinking water are above the World Health Organization (WHO) provisional guideline of 10 $\mu g\,L^{-1}$ (10 ppb) for drinkable water [15]. Many techniques for quantifying such levels of arsenic have been developed, such as atomic adsorption spectrometry, inductively coupled plasma-mass spectrometry, and stripping voltammetry [16–19]. Each method has its respective advantages. The electrochemical method for detecting trace heavy metals has attracted considerable attention in the scientific literature because of its low cost, ease of operation, good sensitivity, and high reproducibility [2,11,16,20,21]. Because it enables accurate measurements of metal ions at $\mu g\,L^{-1}$ level with rapid analysis times, stripping analysis methods, including cathodic and anodic stripping voltammetry, have become popular techniques in this field [7,22–24]. These methods use various electrode materials, including Hg, Pt, Ag, and Au [16,25]. It has been found that Au and Au-nanoparticle-modified electrodes provide a more sensitive anodic current response toward arsenic detection than other electrode materials do. Because of the limited availabilities and high prices of noble metals, many studies have been conducted to investigate minimizing noble-metal loading by reducing the particle size and increasing material utilization [26–29]. The development of sensing techniques using metal nanoparticles is very promising and is becoming an attractive research field in electrochemical detection [1,5,11,24,30–35]. Several different procedures for the synthesis of Au nanoparticles (nAus) have been described, e.g., chemical synthesis, UV or electron beam irradiation, and electrochemical methods [26,34,36–40]. Electrodeposition offers one of the most convenient processes for directly preparing metal catalysts on conductive substrates. However, the deposited sensing materials are essentially limited to the electron conductive

* Corresponding author.
E-mail address: jfh@dragon.nchu.edu.tw (J.-F. Huang).

0039-9140/$ - see front matter © 2013 Elsevier B.V. All rights reserved.
http://dx.doi.org/10.1016/j.talanta.2013.07.063

surface area of the electrode. Accordingly, sensing materials have been prepared and dispersed on solid supports with high surface areas, or within polymers, giving several advantages such as increased nanoparticle capacity, enlargement of the available sensing surface area, improved resistance to interference, and enhancement of stability for materials immobilization [30,34,41,42]. The perfluorosulfonated ionomer, nafion (NF), is an interesting polymer because of its chemical and mechanical stabilities, and its scientific and technological significance [43–45]. Because of their unique cation-exchange ability, from sulfonated groups ($-SO_3^-$), and their biocompatibility, NF films have been used extensively for modifying electrode surfaces and for constructing sensing devices [46–48]. The control of the distribution and microstructure of nAus at the membrane/catalyst interface by electrodeposition is difficult because of issues such as the formation of a dense Au layer and dendritic Au needles during the electrochemical deposition process. In our previous study, a Cu(I)-mediating Pt reduction was proposed and successfully achieved for preparing Pt-nanoparticle-embedded NF catalysts with well-dispersed and protecting-agent-free Pt nanocrystals with a narrow particle size (~2.1 nm) distribution. The catalysts also showed high catalytic performances for facilitation of the oxygen reduction reaction [41]. Here, we will extend Cu(I)-mediating noble-metal reduction (Scheme 1) to the preparation of nAu-embedded NF (NF(Au_{nano})) composites as novel sensing materials for the detection of As(III). Although it has been documented that nAu-modified electrodes are uniquely and highly sensitive in the electrochemical detection of As (III), a major problem associated with the available electrochemical methods is interference from other metal ions, e.g., Cu(II), Hg(II), and so forth, present in natural waters [49,50]. The NF(Au_{nano}) composite combines at least two advantages: the highly dense and uniform distribution of nAus has a highly sensitive response in the electroanalysis of As(III), and the chemically inert and stable binder, NF, provides several additional advantages, including the Donnan effect for cation-preconcentration and increased resistance to interference from other anions and bulky molecules in aqueous solution. To further enhance the selectivity in the detection of As(III), the excellent chelating agent ethylenediaminetetraacetate (EDTA) was added to the sample solution. It has been reported that the complexation constant of the EDTA with these interfering metal ions is much larger than that with As(III) ions [51]. EDTA can selectively chelate with interfering metal ions, forming bulky complexes or bulky anions that are excluded from the NF film (Scheme 2) [52]. The addition of EDTA is expected to effectively increase the selectivity in the detection of As(III).

2. Experimental section

2.1. Reagents

As_2O_3 99.995% (Aldrich), hydrogen tetrachloroaurate trihydrate 99.99% (Alfa), copper nitrate 99.7% (JT-Baker), sodium perchlorate

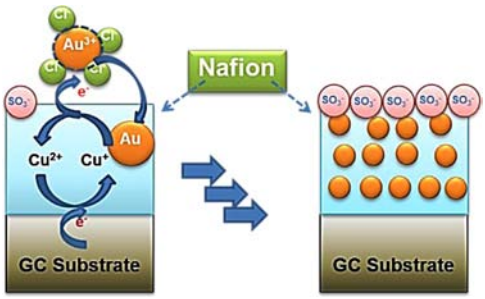

Scheme 1. Schematic of Cu(I)-mediating noble-metal reduction to the preparation of NF(Aunano) composites.

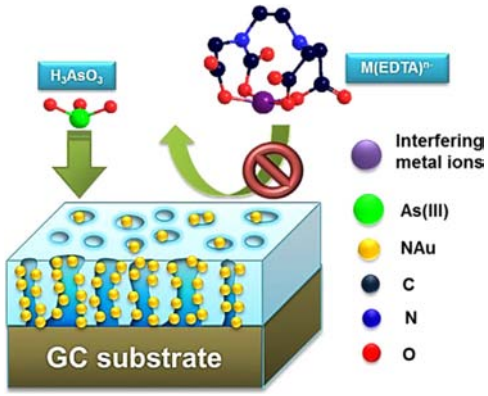

Scheme 2. Schematic of EDTA selectively chelating with interfering metal ions formed bulky complexes or bulky anions that are excluded from the NF film.

(JT-Baker), sulfuric acid (Aldrich), and NF perfluorinated resin (5%) in a mixture of lower aliphatic alcohols and water (Aldrich) were used without purification. All solutions were prepared in deionized water (specific resistivity, 18.2 MΩ cm^{-1}). A stock solution (1000 mg L^{-1}) of As(III) in NaOH was prepared by dissolving the required quantity of As_2O_3, and the pH was adjusted to 5.0 using concentrated HCl. A fresh solution of 0.1 M phosphate buffer (PB; NaH_2PO_4/H_3PO_4, pH 5) containing 0.1 M EDTA stock was prepared daily.

2.2. Fabrication of NF(Au_{nano}) composite

Electrochemical experiments were conducted using a CHI 660C potentiostat/galvanostat. A three-electrode electrochemical cell was used for the electrochemical experiments. Ag/AgCl (3.0 M KCl) and Au wire were used as the reference and counter electrodes, respectively. A glassy carbon (GC) electrode was used as the substrate electrode for the NF membrane or NF(Au_{nano}) composite. The GC electrode was successively polished with 1.0-, 0.3-, and 0.05-μm alumina powder cloths (Buchler), followed by sonication in deionized water (specific resistivity, 18.2 MΩ cm^{-1}), and dried before use. Next, 4.0 μL of 5% NF coating solution was spin-coated onto the GC electrode at 3000 rpm. The GC electrode was covered with a uniform NF thin-film (NF@GC) by evaporating the solvent at room temperature after about 3 min of spinning. The NF(Au_{nano}) composite was obtained by multiple-scan cyclic voltammetry (CV) between 1.0 V and 0.02 V vs. Ag/AgCl (potential range for Cu(II)/Cu (I)) in 0.1 M $NaClO_4$ solution containing 0.1 mM $AuCl_4^-$ and 0.1 mM Cu(II). The scan rate was 50 mV s^{-1} and the temperature was 28 °C. The nAu loading was also controlled by CV sweeping cycles. The nAu mass was evaluated directly from the Cu(II) reduction charge. Specifically, 1 equi. of nAu must be produced to consume 3 equi. of Cu(I). The microstructure of the nAus in the NF(Au_{nano}) composite was observed using a JEOL JEM-1400 transmission electron microscope (TEM). TEM samples were prepared using NF-covered Ti TEM grids (NF@Ti) directly as the working electrode. A Ti grid is used as a conducting substrate to support the NF film because Ti provides ideal polarization behavior, similar to that on the GC substrate in the same potential range. The NF (Au_{nano}) composite was formed directly on the NF@Ti by the same procedure as on the GC substrate. For X-ray diffraction (XRD) measurements (Cu K_α radiation), an indium tin oxide (ITO) glass slide (10 mm × 10 mm) was used as the substrate for the NF (Au_{nano}) composite. The ITO glass slide was sonicated in acetone and ethanol solutions for 20 min, sequentially rinsed with deionized water (specific resistivity 18.2 MΩ cm^{-1}), and dried in an oven before being used as the working electrode. Next, 5% NF was dip-coated onto the ITO glass slide. A uniform NF thin-film was deposited on the ITO glass slide (NF@ITO) by evaporation in air at

room temperature after about 30 min. The NF(Au_{nano}) composite was formed on the NF@ITO by the same procedure as on the GC substrate.

2.3. Electrochemical measurements

An NF(Au_{nano})-composite-covered GC (NF(Au_{nano})@GC) was used as the working electrode for As(III) determination. The as-prepared working electrode was electrochemically cleaned using a cycling potential between 0.0 and 1.5 V (vs. Ag/AgCl), 30 times, in Ar-purged 0.5 M sulfuric acid. The electrochemical surface area (ECSA) (or microscopic surface area, A_m) was estimated from the integrated reduction current of gold oxide and a conversion factor of 390 μC cm^{-2} [53]. The roughness factor (R_f) and the specific ECSA (ECSA/nAu loading, $m^2\ g^{-1}$) were directly calculated from the ECSA. The R_f is the ratio of the microscopic surface area, A_m, and the geometric area, A_g, of the polished gold electrode [53].

The freshly prepared NF(Au_{nano})@GC was dipped in a stirred analyte solution containing As(III) and kept at −0.6 V vs. Ag/AgCl for the time required for preconcentration (120 s). Quantitative determinations were then performed in the square-wave voltammetry (SWV) mode. The potential was scanned in the anodic direction from −0.6 to 0.5 V vs. Ag/AgCl. A medium containing 0.1 M EDTA and 0.1 M PB buffer (pH=5.0) was used in the electrochemical experiments. Solutions and samples were analyzed with 5 min deoxygenation. After recording the voltammogram, the electrode was regenerated by immersing it in bare 0.1 M EDTA and 0.1 M PB buffer at 0.5 V vs. Ag/AgCl for 30 s. The renewed electrode was then checked in the supporting electrolyte before the next measurement to ensure that it did not show any peaks within the potential range. Groundwater from the southern area of Taiwan, drinking water, and lake water were collected from the campus of National Chung-Hsing University in Taiwan and stored in pre-cleaned polyethylene bottles after filtration. The standard addition method was used to evaluate the As(III) content in the water samples.

3. Results and discussion

CVs of Cu(II) on an NF@GC electrode, recorded in the reversed potential preceding the bulk deposition of Cu in a 0.1 M $NaClO_4$ solution containing 0.1 mM Cu(II) are shown in Fig. 1A. The Cu(II) reduction process involves the transfer of two consecutive electrons, with Cu(I) as a soluble intermediate (Fig. S1). A pair of shoulder redox waves (c_1'/a_1') arose from a reversible reaction, Cu(II)+e^- ↔Cu(I) [54]. In our previous study, it was demonstrated that the cationic property of Cu(II) enables effective accumulation in NF@GC [41]. The effect of $AuCl_4^-$ on the redox behavior of Cu(II)/Cu(I) on the NF@GC electrode is shown in Fig. 1A. Typical redox waves for Cu(II)/Cu(I) on NF@GC were observed in the absence of $AuCl_4^-$. However, the reduction current of the forward scan significantly increased, and the oxidation current of the returning scan disappeared and was replaced by a continual reduction current after the addition of $AuCl_4^-$ to the solution. In addition, the starting reduction potential of Cu(II) was also positively shifted from ~50 mV to ~200 mV. This behavior is similar to a typical EC′ catalytic process [53]. For comparison, CVs of 0.1 mM $AuCl_4^-$ were recorded on bare GC and NF@GC electrodes in the same electrolyte solution without Cu(II), and are shown in the inset of Fig. 1A. An obviously cathodic current for the reduction of Au(III) to Au(I) was observed on the bare GC electrode but was completely inhibited on the NF@GC electrode. It is due to $AuCl_4^-$ was limited to penetrate within the NF modified layer by the negative Donnan effect. The possible mechanism is shown in Scheme 1. This behavior could be ascribed to the reduction of Cu(II) to Cu(I) in the cathodic potential scan. The as-formed Cu(I) accumulated in the NF modified layer. The accumulated Cu(I) serves as a movable mediator in the NF. The Cu(I) was chemically re-oxidized back to

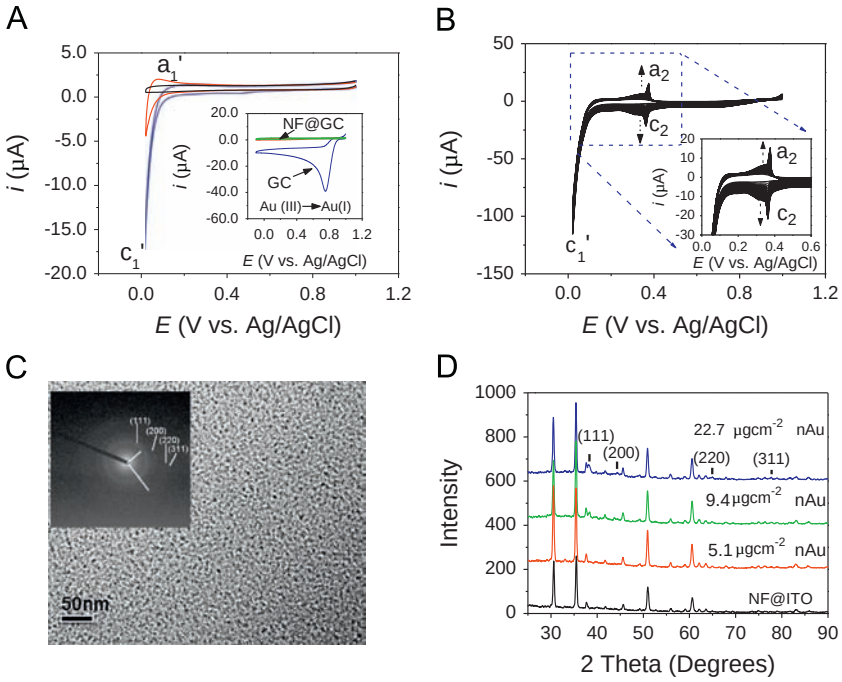

Fig. 1. (A) CVs of 0.1 mM Cu(II) recorded on an NF@GC electrode in 0.1 M $NaClO_4$ aqueous solution (blue line) with 0.1 mM $AuCl_4^-$ and (red line) without $AuCl_4^-$. The blank CV on an NF@GC electrode in 0.1 M $NaClO_4$ aqueous solution is shown as a black line. The inset shows CVs of 0.1 mM $AuCl_4^-$ on (red line) the NF@GC and (blue line) the bare GC in 0.1 M $NaClO_4$ aqueous solution. A blank CV of 0.1 M $NaClO_4$ aqueous solution on the NF@GC is shown as a green line. (B) A multiple-scan CV recorded on NF@GC in 0.1 M $NaClO_4$ solution containing 0.1 mM Au(III) and 0.1 mM Cu(II). The inset is a magnified figure in the potential range from 0.6 V to 0.0 V. (C) TEM image of NF(Au_{nano})@Ti and a selected area electron direction pattern. (D) XRD patterns (Cu K_α) of a series of NF(Au_{nano})@ITO slides with various nAu loadings, and the bare NF@ITO substrate. (For interpretation of the references to color in this figure legend, the reader is referred to the web version of this article.)

Cu(II) by $AuCl_4^-$ as a result of diffusion of Cu(I) to the interface between NF and the $AuCl_4^-$ solution. The specific EC′ catalytic process is expected to reduce $AuCl_4^-$ to Au. The chemically regenerated Cu(II) was reduced to Cu(I) immediately at the electrode surface, thereby repeatedly contributing to inducing formation of zero-valence Au in the NF modified layer. In order to study this proposed mechanism, a multiple-scan CV of Cu(II) in 0.1 M $NaClO_4$ solution containing both 0.1 mM Au(III) and 0.1 mM Cu(II) on the NF@GC electrode was recorded, as shown in Fig. 1B. In addition to the cathodic reduction wave, c_1', a new pair of symmetric redox waves, c_2/a_2, gradually grew up during the repeated potential scans. These as-growth symmetric redox waves corresponded to underpotentially deposited (UPD) Cu and subsequent stripping of the Cu monolayer on the Au surface [33]. This indicated that Au was formed and the Au loading was increased, gradually increasing the ECSA of Au during the repeated potential scans. TEM was used to characterize the micro-morphology of the product from the Cu(I)-mediating Au reduction reaction in the NF (Au_{nano}) composite (Fig. 1C). Interestingly, the TEM image shows that highly dense nAus with nearly spherical shapes were well dispersed in the NF film, with a narrow size distribution of 4.4–5.2 nm (Fig. S2). The electron diffraction (ED) pattern of the NF (Au_{nano}) composite was recorded at three randomly sampled points on the NF(Au_{nano}) surface. The ED pattern revealed that the nAus have (111), (200), (220), and (311) Au crystalline facets (Fig. 1C). The repeatable ED pattern indicated that nAus uniformly distributed in the NF(Au_{nano}) composite. The crystallinity and purity of the as-prepared NF(Au_{nano}) composite were investigated by XRD. The NF(Au_{nano}) composite was obtained on an NF@ITO as a working electrode by multiple-scan CV (potential range: 1.0–0.05 V). XRD analyses of the composites indicated that they contained Au with no traces of other elements other than a background signal from the ITO substrate (Figs. 1D and S2). The XRD pattern of the NF(Au_{nano}) composite showed four peaks corresponding to the (111), (200), (220), and (311) planes of a face-centered cubic lattice of Au. The intensities of the characteristic peaks of Au increased with increasing Au loading in the NF (Au_{nano}) composite. The peaks were broad, indicating a small crystal size of the embedded nAus. The size of the nAus was calculated from X-ray line-broadening analysis, using the Scherrer formula [55]. The size was calculated to be about 5.4 nm, which was consistent with the TEM image.

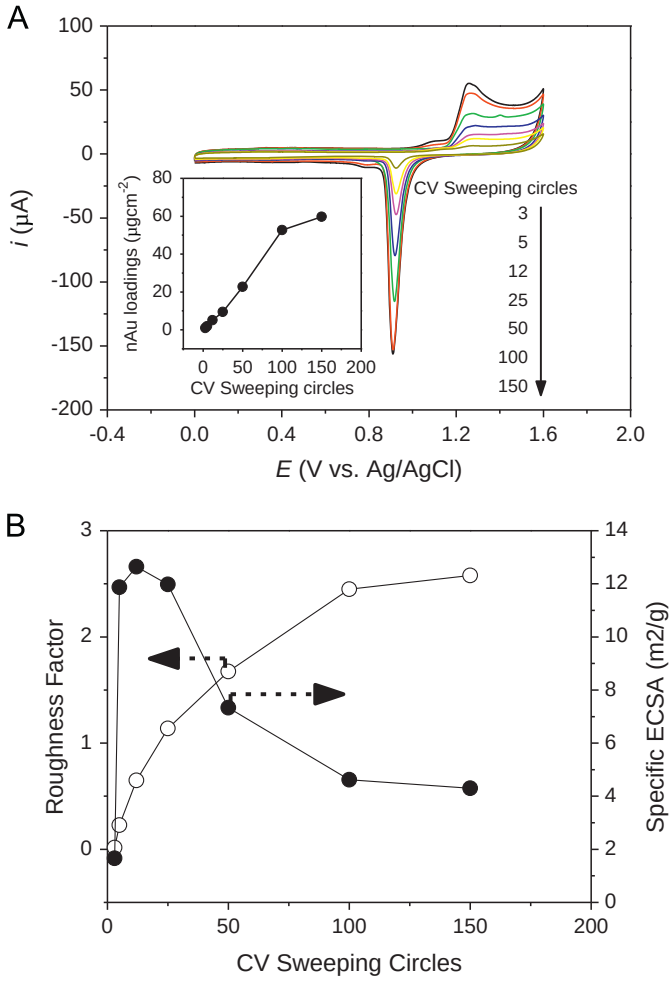

Fig. 2. (A) CVs recorded in 0.5 M H_2SO_4 for a series of NF(Au_{nano})@GC electrodes. Inset is nAu loading in NF(Au_{nano}) composite vs. sweeping cycles in the Cu(I)-mediating Au reduction reaction. (B) Roughness factor (○) and specific ECSA (●) of NF(Au_{nano}) composite vs. sweeping cycles in the Cu(I)-mediating Au reduction reaction.

So far, we have demonstrated that the NF(Au_{nano}) composite was simply obtained by multiple-scan CV. The nAu loading was also controlled by the CV sweeping cycles. The ECSA is an important factor for potential applications such as catalysis and electroanalysis. The CVs of NF(Au_{nano})@GC electrodes with various nAu loadings, recorded in 0.2 M H_2SO_4 at 200 mV s^{-1} from 1.5 V to 0.0 V (vs. Ag/AgCl), are shown in Fig. 2A. Different loadings were achieved by varying the number of CV sweeping cycles in the Cu(I)-mediating Au reduction reaction. These voltammograms show current peaks from the formation of surface gold oxide in the anodic scan and subsequent gold oxide reduction in the cathodic scan. The ECSA was evaluated from the integrated reduction current of the gold oxide [53]. The result indicated that the ECSA increased with increasing nAu loading, from the significant enhancement of the reduction charge of the gold oxide (Fig. 2A). The ECSA of the NF(Au_{nano}) composite ranges from 1.6×10^{-2} to 1.8×10^{-1} cm^2. This is much larger than the ECSA of nAus directly electrodeposited on the electrode surface without NF (from 8.6×10^{-4} to 2.6×10^{-2} cm^2) [25]. In order to gain an insight into the ECSA of the NF(Au_{nano}) composite, the R_f and the specific ECSA (ECSA/nAu loading, $m^2\ g^{-1}$) can also be directly calculated from the ECSA. These two factors are significant for realizing the surface roughness and catalytic activity of the catalytic material covering the electrode surface (Fig. 2B). The R_f of the NF(Au_{nano}) composite gradually increased with the number of CV sweeping cycles in the Cu(I)-mediating Au reduction reaction, and then leveled off at about 2.5. Since the number of CV sweeping cycles was more than 50 (nAu loading 9.4 μg cm^{-2}), the R_f reached a limiting plateau. The largest specific ECSA (12.6 $m^2\ g^{-1}$) was reached at about 25 cycles (nAu loading 5.1 μg cm^{-2}) and began to decrease above 50 cycles (nAu loading 9.4 μg cm^{-2}). These results indicate that the NF(Au_{nano}) composite not only provides a greatly increased specific ECSA, but that it also has a weak influence on the electrode surface roughness under very low nAu loadings.

The utility of the NF(Au_{nano}) composite was tested by the detection of As(III) in aqueous solutions. To examine the performance of the NF (Au_{nano}) composite in As(III) detection in aqueous solutions (Fig. 3A), the electrochemical response toward As(III) was first examined using CVs recorded on NF@GC and NF(Au_{nano})@GC (nAu loading 9.4 μg cm^{-2}) electrodes, in a 0.1 M PB buffer solution containing 0.1 M EDTA and 0.5 mg L^{-1} As(III) (pH 5.0). It is clear that As(III) was selectively detected only on the NF(Au_{nano})@GC electrode, since no response was observed on the NF@GC electrode. The broad cathodic peak observed at −0.40 V (Fig. 3A) during the negative sweep is assigned to the reduction of As(III) to As, whereas the sharp symmetric anodic stripping peak observed at −0.03 V during the reverse positive sweep corresponds to the reoxidation of As to water-soluble As(III). The NF modified layer was successfully functionalized with unique activity for the detection of As(III) after embedding of nAus.

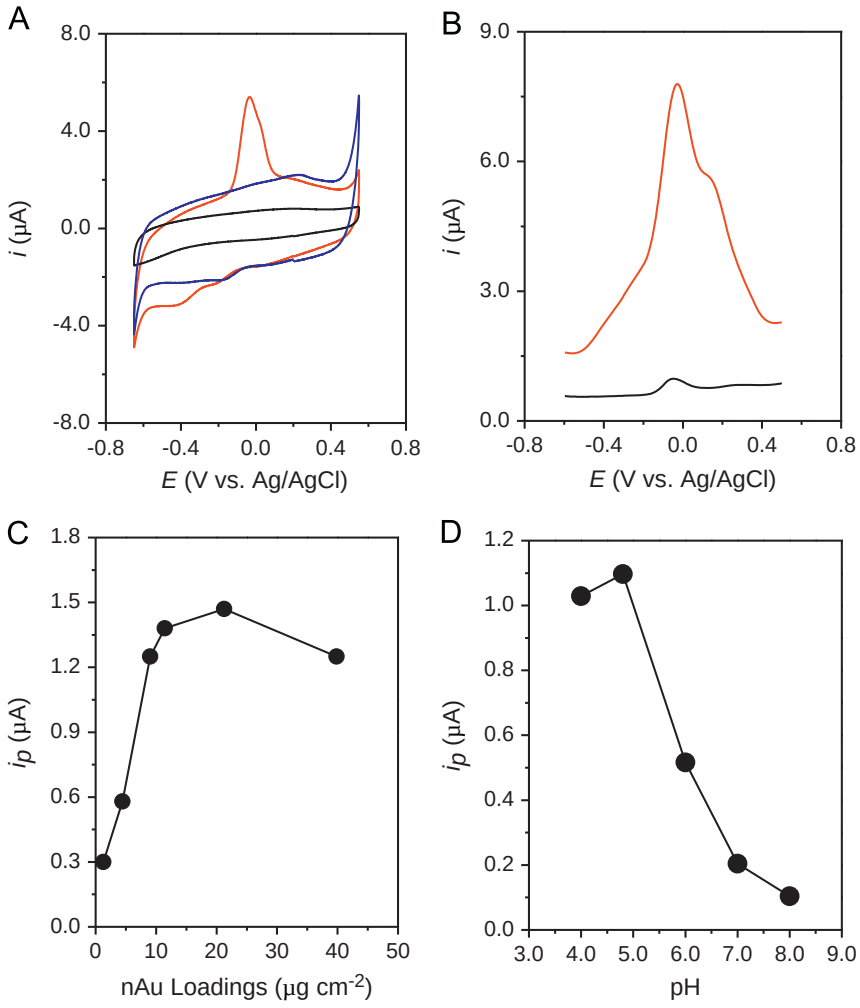

Fig. 3. (A) CVs of 0.5 mg L^{-1} As(III) recorded on (red line) NF(Au_{nano})@GC (nAu loading 9.4 μg cm^{-2}) and (black line) bare GC electrodes in 0.1 M PB solution (pH 5.0) containing 0.1 M EDTA. A blank CV of 0.1 M PB solution (pH 5.0) containing 0.1 M EDTA on the NF(Au_{nano})@GC (nAu loading 9.4 μg cm^{-2}) is shown as a blue line. (B) SWASV responses of 10 μg L^{-1} As(III) in 0.1 M PB solution (pH 5.0) containing 0.1 M EDTA recorded on (red line) NF(Au_{nano})@GC (nAu loading 9.4 μg cm^{-2}) and (black line) NF@Au electrodes. (C) Dependence of SWASV peak current of 10.0 μg L^{-1} As(III) in 0.1 M PB solution (pH 5.0) containing 0.1 M EDTA solution on nAu loading in NF(Au_{nano})@GC composite. (D) Dependence of SWASV peak current of 10.0 μg L^{-1} As(III) in 0.1 M PB solution containing 0.1 M EDTA solution on pH, for As(III) determination obtained on NF (Au_{nano})@GC electrode (nAu loading 9.4 μg cm^{-2}). (For interpretation of the references to color in this figure legend, the reader is referred to the web version of this article.)

The detection sensitivity was further improved by using the more sensitive square-wave anodic stripping voltammetry (SWASV) (Fig. 3B). The detection of As(III) using SWASV involves two steps: (i) cathodic deposition of As at an optimized potential (E_{dep}, −0.6 V) for a duration time (120 s), and (ii) anodic stripping of the deposited As. The peak current was compared with those of an NF-covered macro-disc gold electrode (NF@Au) and the NF (Au_{nano})@GC electrode. As shown in Fig. 3B, The SWASV peak current of 10 μg L^{-1} As(III) at the NF(Au_{nano})@GC electrode is about 20 times higher than that obtained at the NF@Au electrode. It is clear that the NF(Au_{nano})@GC electrode has a much higher sensitivity toward As(III) as a result of its large specific ECSA.

In order to obtain the optimum conditions for the determination of As(III), two significant system variables, i.e., the nAu loading in the NF (Au_{nano}) composite and the pH of the As(III) solution, were selected for optimization to improve the analytical performance. It can be seen that increasing the nAu loading led to an increase in the SWASV peak current of 10.0 μg L^{-1} As(III). The peak current reached a maximum value and then gradually decreased when the nAu loading was over 9.4 μg cm^{-2} (Fig. 3C). A similar trend is observed in Fig. 2B. The loss of sensitivity could be the result of increasing the nAu loading too much, causing a decrease of the specific ECSA of the NF(Au_{nano}) composite.

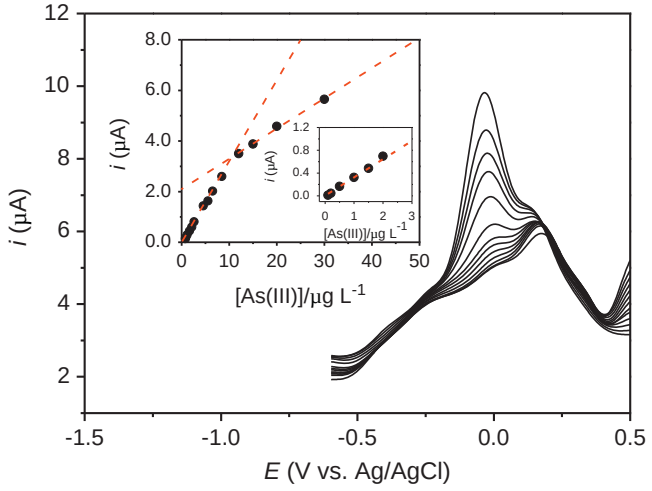

Fig. 4. Typical SWASVs for the detection of As(III) on NF(Au_{nano})@GC electrode (nAu loading 9.4 μg cm^{-2}) in 0.1 M PB aqueous solution with 0.1 M EDTA containing 0.1, 0.2, 0.5, 1.0, 1.5, 2.0, 4.0, 6.0, 8.0, 12.0, 15.0, 20.0, and 30.0 μg L^{-1} As(III) for 5 min of preconcentration time. E_{dep} is −0.6 V. Inset: calibration curve of the SWASV peak current vs. the concentration of As(III), from 0.1 to 30.0 μg L^{-1}.

The optimum condition for As(III) accumulation was observed when the sample solution was slightly acidic (pH ≤ 5.0), as shown in Fig. 3D. As(III) speciation is complicated as it is normally considered as an oxyanion. Calculation of the As(III) speciation as a function of pH showed (Fig. S4A) that the major As(III) species should be neutral H_3AsO_3 at pH < 7.0 [56]. In a basic solution, the de-protonation speciation of H_3AsO_3, giving $H_2AsO_3^-$, $HAsO_3^{2-}$, and AsO_3^{3-}, should be limited in NF by the negative Donnan effect. In more acidic solutions, the SO_3^- sites of NF attracted more proton ions on the electrode surface and the neutral H_3AsO_3 freely accumulated in NF. In further considering the selectivity, the excellent chelating abilities of EDTA were used to reduce interference from metal ions. EDTA is a well-known and widely used chelator in analytical chemistry [57]. In too-acidic solutions, a hexaprotic ion, designated H_6Y^{2+}, is the major EDTA species, and its chelating ability with metal ions is lost. Calculation of the EDTA speciation as a function of pH showed (Fig. S4B) that the major EDTA species formed H_2Y^{2-}, HY^{3-}, and Y^{4-}, which chelate more strongly with metal ions in aqueous solutions of pH > 4.0. To give good sensitivity and selectivity, and to reduce the Au loading, in the detection of As(III), pH 5 was selected as the optimum pH and the nAu loading was controlled at about 9.4 μg cm^{-2}.

Calibration data were obtained under the optimized experimental conditions mentioned above. Fig. 4 shows some typical SWASV voltammograms for the NF(Au_{nano})@GC electrode at different As(III) concentrations. In all cases, a stripping response was observed at a potential in the vicinity of −0.03 V vs. Ag/AgCl. A calibration graph was then constructed from the observed peak currents (inset of Fig. 4). The graph showed a dynamic range from 0.1 to 12.0 μg L^{-1} (from 1.3 to 160 nM). The dynamic range of the calibration curve, $y = 23.98x$ (in μA μM^{-1})+0.42 ($R^2 = 0.999$), showed linear behavior with a slope (sensitivity) of 23.98 μA μM^{-1}. The detection limit, equal to three times the standard deviation of the background, was 0.047 μg L^{-1} (0.63 nM). This detection limit is comparable to or better than the detection limits offered by previous reports at a poly-Au electrode (13.7 μg L^{-1}) using the same method of detection [58]. As the detection limit is well below the guideline value for As(III) in

Table 1
Interference studies at the NF(Au_{nano})@GC electrode in the presence of EDTA in the detection of As (III).

Ions	Concentration/μg L^{-1}	SWASV peak current/μA	Relative difference from 10 μg L^{-1} As(III)
As^{3+}	10	2.95	0.00
Cu^{2+}	1000	2.98	0.01
Hg^{2+}	1000	2.93	−0.01
Pb^{2+}	1000	2.90	−0.02
Fe^{3+}	1000	2.89	−0.02
Co^{2+}	1000	2.85	−0.03
Ni^{2+}	1000	2.91	−0.01
Zn^{2+}	1000	2.91	−0.01
Sn^{2+}	1000	2.95	0.00
Bi^{3+}	1000	2.90	−0.02
Cd^{2+}	1000	2.84	−0.04

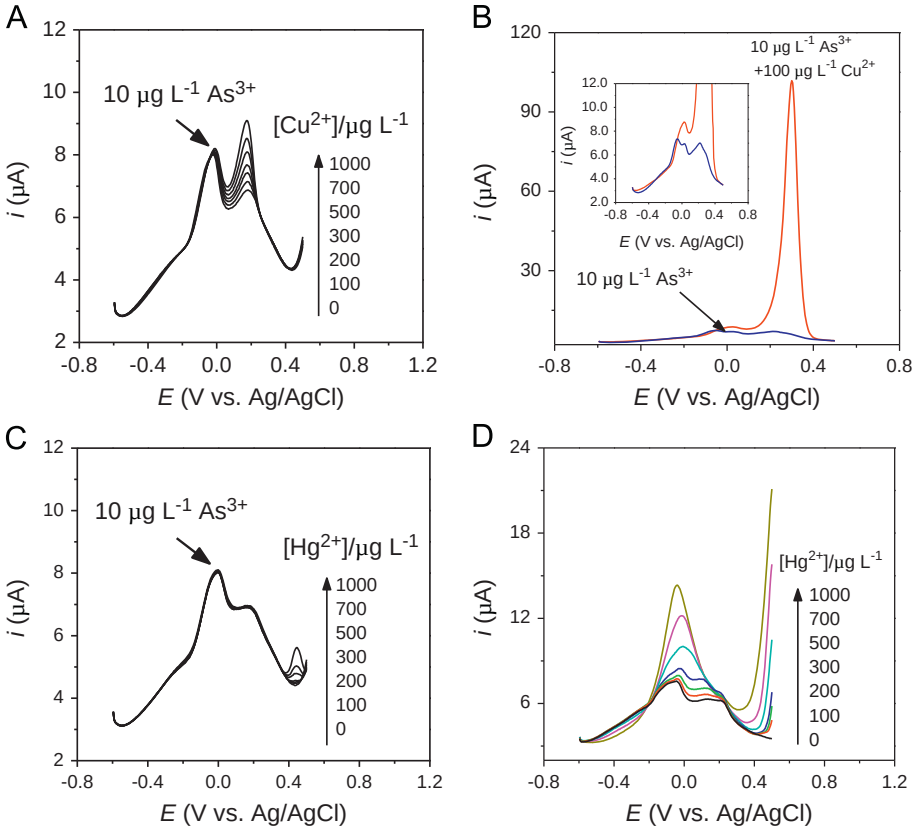

Fig. 5. SWASVs obtained at the NF(Au_{nano})@GC electrode for a 10.0 μg L^{-1} As (III) in 0.1 M PB solution in the presence of various concentration of (A)(B) Cu(II), and (C)(D) Hg (II). (A)(C) with EDTA, (B)(D) without 0.01 M EDTA. The pH of the solution was 5.0.

Table 2
Measurement of As (III) on a groundwater, lake water, and drinking water.

Sample*	Detected value, original ($\mu g\ L^{-1}$)	Spike ($\mu g\ L^{-1}$)	Detected value after spiking ($\mu g\ L^{-1}$)	Recovery (%)
SATW-1**	5.04**	5.0	10.1	101.2
Lake water	ND	5.0	5.1	102.0
Drinking water	ND	5.0	5.0	100.0

* Number of measurements, 5.
** The certified value is 5.04 $\mu g\ L^{-1}$; the aqueous sample is from groundwater in the southern part of Taiwan.

drinking water set by the WHO, the NF(Au_{nano})@GC electrode is suitable for real sample analysis.

Various ions were examined regarding their interference in the determination of As(III). The use of the NF(Au_{nano})@GC electrode with EDTA in the sample solution successfully eliminated such interference. For 10.0 $\mu g\ L^{-1}$ As(III), the results showed that an over 100-fold excess concentration of Cu(II), Hg(II), Pb(II), Fe(III), Co(II), Ni(II), Zn(II), Sn(II), Bi (III), and Cd(II) can be tolerated (Table 1). Note that Cu(II) and Hg(II) are generally considered to be the major interfering metals in the determination of As(III) in a typical voltammetric analysis. This problem can be greatly alleviated using the proposed procedure, as indicated above. To examine the analytical performance of EDTA addition in terms of As(III) detection, the major interfering metal ions, Cu(II) and Hg(II), were selected as typical examples. Fig. 5A and C show voltammograms obtained in the presence of 0.1 M EDTA; the SWASV peak currents were recorded for 10.0 $\mu g\ L^{-1}$ As(III) with the addition of different concentrations of Cu(II) and Hg(II) ($100-1000\ \mu g\ L^{-1}$). The peak observed at -0.03 V corresponds to the anodic oxidation of As, whereas the peaks at 0.2 V and 0.45 V arise from the oxidation of Cu and Hg, respectively. The position and current of the stripping peak of As(III) did not change during the addition of interfering ions. In the absence of EDTA, serious interference by these metal ions was clearly observed (Fig. 5B and D). The current of the stripping peak of As(III) was completely covered by the much stronger signal from the oxidation of Cu. Although the signal from the oxidation of Hg did not directly cover the analytical response of As(III), the addition of Hg (II) caused the analytical response of As(III) to change significantly as a result of the formation of amalgam during the process of cathodic deposition of As.

After recording the voltammogram, the electrode was regenerated by immersing it in bare 0.1 M EDTA and 0.1 M PB buffer at 0.5 V vs. Ag/AgCl for 30 s. The renewed electrode was then checked in the supporting electrolyte before the next measurement to ensure that it did not show any peaks within the potential range. This method showed an excellent reproducibility of the measurements, usually around 1.2% in terms of percent relative standard deviation for eight repetitive preconcentration-stripping-renewal experiments.

The analysis of real samples using the NF(Au_{nano})@GC electrode was assessed by using it to determine As(III) in groundwater from the southern part of Taiwan, lake water, and drinking water (Taichung, Taiwan). The results are summarized in Table 2 and indicate good accuracy for all the samples. The real values for the As(III) contents in these samples were calculated from the dilution factors (10-fold) for each sample during preparation.

4. Conclusions

In conclusion, a facile approach for fabricating the NF(Au_{nano}) composite composed of well-dispersed, highly dense, and protecting-agent-free Au nanocrystals with a uniform and narrow particle size distribution was developed. We also demonstrated the controllable growth rate of nAu by diffusion of a Cu(I) mediator and the intrinsic stabilizer-NF modified layer in our newly developed method. A highly sensitive and selective method for the determination of As(III) was also described using the NF(Au_{nano})@GC electrode with a low Au loading as a sensing probe. The results showed that the SWASV determination of trace As(III), based on the NF(Au_{nano})@GC electrode in the presence of EDTA, is simple and effective. The proposed procedure not only yields good sensitivity but also offers improved resistance to metal ions interferences, especially from Cu(II) and Hg(II). We believe that this new material has the potential to be extended to a wide range of related applications, including in the energy and sensing fields.

Acknowledgment

This work was supported by the National Science Council of the Republic of China, Taiwan.

Appendix A. Supplementary material

Supplementary data associated with this article can be found in the online version at http://dx.doi.org/10.1016/j.talanta.2013.07.063.

References

[1] G. Aragay, J. Pons, A. Merkoci, Chem. Rev. 111 (2011) 3433–3458.
[2] C. Kokkinos, A. Economou, Curr. Anal. Chem. 4 (2008) 183–190.
[3] J. Wang, Electroanalysis 17 (2005) 1341–1346.
[4] Y. Yardim, Rev. Anal. Chem. 30 (2011) 37–43.
[5] J.F. Huang, B.T. Lin, Analyst 134 (2009) 2306–2313.
[6] B.K. Jena, C.R. Raj, Anal. Chem. 80 (2008) 4836–4844.
[7] J. Wang, Acc. Chem. Res. 35 (2002) 811–816.
[8] L. Xiao, G.G. Wildgoose, R.G. Compton, Anal. Chim. Acta 620 (2008) 44–49.
[9] X. Cheng, J. Li, X. Li, D. Zhang, H. Zhang, A. Zhang, H. Huang, J. Lian, J. Mater. Chem. 22 (2012) 24102–24108.
[10] R. Feeney, S.P. Kounaves, Anal. Chem. 72 (2000) 2222–2228.
[11] D.E. Mays, A. Hussam, Anal. Chim. Acta 646 (2009) 6–16.
[12] D. Melamed, Anal. Chim. Acta 532 (2005) 1–13.
[13] M.R. Rahman, T. Okajima, T. Ohsaka, Anal. Chem. 82 (2010) 9169–9176.
[14] M.K. Sengupta, M.F. Sawalha, S.I. Ohira, A.D. Idowu, P.K. Dasgupta, Anal. Chem. 82 (2010) 3467–3473.
[15] WHO, World Health Organization, 2001.
[16] D.Q. Hung, O. Nekrassova, R.G. Compton, Talanta 64 (2004) 269–277.
[17] M.R. Karagas, T.D. Tosteson, J.D. Blum, B. Klaue, J.E. Weiss, V. Stannard, V. Spate, J.S. Morris, Am. J. Epidemiol. 152 (2000) 84–90.
[18] B. Klaue, J.D. Blum, Anal. Chem. 71 (1999) 1408–1414.
[19] M. Leermakers, W. Baeyens, M. De Gieter, B. Smedts, C. Meert, H.C. De Bisschop, R. Morabito, P. Quevauviller, Trac-Trends Anal. Chem. 25 (2006) 1–10.
[20] J. Gong, T. Zhou, D. Song, L. Zhang, X. Hu, Anal. Chem. 82 (2010) 567–573.
[21] W. Qin, R. Liang, X. Fu, Q. Wang, T. Yin, W. Song, Anal. Chem. 84 (2012) 10509–10513.
[22] T.M. Florence, Analyst 111 (1986) 489–505.
[23] S.M. Skogvold, O. Mikkelsen, Electroanalysis 20 (2008) 1738–1747.
[24] K.E. Toghill, G.G. Wildgoose, A. Moshar, C. Mulcahy, R.G. Compton, Electroanalysis 20 (2008) 1731–1737.
[25] X. Dai, O. Nekrassova, M.E. Hyde, R.G. Compton, Anal. Chem. 76 (2004) 5924–5929.
[26] S.J. Guo, E.K. Wang, Nano Today 6 (2011) 240–264.
[27] K. Sasaki, H. Naohara, Y. Cai, Y.M. Choi, P. Liu, M.B. Vukmirovic, J.X. Wang, R. R. Adzic, Angew. Chem. Int. Ed. 49 (2010) 8602–8607.
[28] J.F. Huang, H.Y. Chen, Angew. Chem. Int. Ed. 51 (2012) 1684–1688.
[29] J.N. Anker, W.P. Hall, O. Lyandres, N.C. Shah, J. Zhao, R.P. Van Duyne, Nat. Mater. 7 (2008) 442–453.
[30] J.F. Huang, Talanta 77 (2009) 1694–1700.
[31] L. Rassaei, M. Sillanpaeae, R.W. French, R.G. Compton, F. Marken, Electroanalysis 20 (2008) 1286–1292.
[32] J. Orozco, C. Fernandez-Sanchez, C. Jimenez-Jorquera, Environ. Sci. Technol. 42 (2008) 4877–4882.
[33] J.F. Huang, Electroanalysis 20 (2008) 2229–2234.
[34] J.F. Huang, Chem. Commun. (2009) 1270–1272.
[35] J.-F. Huang, M.-C. Fan, J. Mater. Chem. 20 (2010) 1431–1434.
[36] M.C. Daniel, D. Astruc, Chem. Rev. 104 (2004) 293–346.
[37] T. Panda, K. Deepa, J. Nanosci. Nanotechnol. 11 (2011) 10279–10294.
[38] K. Saha, S.S. Agasti, C. Kim, X. Li, V.M. Rotello, Chem. Rev. 112 (2012) 2739–2779.

[39] S. Tokonami, Y. Yamamoto, H. Shiigi, T. Nagaoka, Anal. Chim. Acta 716 (2012) 76–91.
[40] L. Vigderman, B.P. Khanal, E.R. Zubarev, Adv. Mater. 24 (2012) 4811–4841.
[41] J.-F. Huang, W.-R. Chang, J. Mater. Chem. 22 (2012) 17961–17966.
[42] X. Dai, G.G. Wildgoose, C. Salter, A. Crossley, R.G. Compton, Anal. Chem. 78 (2006) 6102–6108.
[43] C.Y. Wang, Chem. Rev. 104 (2004) 4727–4765.
[44] S. Hrapovic, Y.L. Liu, K.B. Male, J.H.T. Luong, Anal. Chem. 76 (2004) 1083–1088.
[45] M.N. Szentirmay, C.R. Martin, Anal. Chem. 56 (1984) 1898–1902.
[46] Q. Gao, Y.Y. Guo, J. Liu, X.Q. Yuan, H.L. Qi, C.X. Zhang, Bioelectrochemistry 81 (2011) 109–113.
[47] K.J. Chen, C.F. Lee, J. Rick, S.H. Wang, C.C. Liu, B.J. Hwang, Biosens. Bioelectron. 33 (2012) 75–81.
[48] J. Wang, M. Musameh, Y.H. Lin, J. Am. Chem. Soc. 125 (2003) 2408–2409.
[49] X. Dai, R.G. Compton, Analyst 131 (2006) 516–521.
[50] G.M.S. Alves, J. Magalhaes, P. Salaun, C.M.G. van den Berg, H. Soares, Anal. Chim. Acta 703 (2011) 1–7.
[51] Martell AE, Smith RM, Motekaities RJ., MD, 2001.
[52] T. Mizuta, J. Wang, K. Miyoshi, Bull. Chem. Soc. Jpn. 66 (1993) 2547–2551.
[53] A.J. Bard, L.R. Faulkner, Electrochemical Method: Fundamentals and Applications, 2nd ed., John Wiley & Son, New York, 2001.
[54] R. Drissi-Daoudi, A. Irhzo, A. Darchen, J. Appl. Electrochem. 33 (2003) 339–343.
[55] B.D. Cullity, Elements of X-ray Diffraction, Addision-Wesley, Reading, MA, 1978.
[56] M. Sadiq, T.H. Zaidi, A.A. Mian, Water Air Soil Pollut. 20 (1983) 369–377.
[57] D.C. Harris, Quantitative Chemical Analysis, 8th ed., W.H. Freeman and Company, New York, 2008.
[58] A.O. Simm, C.E. Banks, R.G. Compton, Electroanalysis 17 (2005) 1727–1733.